International Journal of Geo-Information

MDPI

Article

Ownership Protection on Digital Elevation Model (DEM) Using Transform-Based Watermarking

Fahmi Amhar [1], Endang Purnama Giri [2], Florence Elfriede Sinthauli Silalahi [3,*], Shelvie Nidya Neyman [2], Anggrahito [4], Dadan Ramdani [3,5], Danang Jaya [4], Dewayany Sutrisno [1], Sandi Adhitya Kolopaking [1], Tia Rizka Nuzula Rachma [1] and Murdaningsih [1]

[1] Badan Informasi Geospasial—Geospatial Information Agency of Indonesia, West Java 16911, Indonesia; fahmi.amhar@big.go.id (F.A.); dewayany@big.go.id (D.S.); sandi.adhitya@big.go.id (S.A.K.); tia.rizka@big.go.id (T.R.N.R.); murdaningsih@big.go.id (M.)
[2] Computer Sciences Department, Faculty of Mathematics and Natural Sciences, IPB University, West Java 16680, Indonesia; endangpurnamagiri@apps.ipb.ac.id (E.P.G.); shelvie@apps.ipb.ac.id (S.N.N.)
[3] Badan Riset dan Inovasi Nasional Republik Indonesia—The National Research and Innovation Agency, West Java 16911, Indonesia; dada033@brin.go.id
[4] The National Cyber and Crypto Agency of Indonesia, DKI Jakarta 12550, Indonesia; anggrahito@bssn.go.id (A.); danang.jaya@bssn.go.id (D.J.)
[5] Geodesy Department, Faculty of Engineering, Universitas Pakuan, West Java 16143, Indonesia
* Correspondence: flor006@brin.go.id

Abstract: This research aims to protect Digital Elevation Model (DEM) data from piracy or counterfeiting. An invisible watermark inserted into the data, which will not considerably change the data value, is necessary. The proposed method involves the use of the two-dimensional discrete cosine transform (2D DCT), a combination of 2D DCT and discrete wavelet transform (DWT), and two-dimensional discrete Fourier transform (2D DFT) in the frequency domain. The data used include a National DEM file downloaded from the geoportal of the Geospatial Information Agency (*Badan Informasi Geospasial*—BIG). Three files represent mountainous, lowland/urban, and coastal areas. An "attack" is also conducted on the watermarked DEM by cropping. The results indicate that the watermarked DEM is well recognized. The watermark can be read 100% for 2D DCT, while that for 2D DFT can be read 90.50%. The distortion value of the elevation data under the DCT technique demonstrates the smallest maximum value of 0.1 m compared with 4.5 and 1.1 m for 2D DFT and 2D DCT–DWT. Meanwhile, the height difference (Max Delta), the peak signal-to-noise ratio, and the root mean squared error (RMSE) are highest in mountainous, lowland, and coastal areas, respectively. Overall, the 2D DCT is also superior to the 2D DFT and the2D DCT–DWT. Although only one can recognize the nine watermarks inserted on each sheet, DEMs attacked by the cropping process can still be identified. However, this finding can sufficiently confirm that DEMs belong to BIG.

Keywords: data protection; digital elevation model (DEM); discrete cosine transform; discrete Fourier transform; discrete wavelet transform; GeoTIFF; ownership; watermarking

Citation: Amhar, F.; Giri, E.P.; Silalahi, F.E.S.; Neyman, S.N.; Anggrahito; Ramdani, D.; Jaya, D.; Sutrisno, D.; Kolopaking, S.A.; Rachma, T.R.N.; Murdaningsih. Ownership Protection on Digital Elevation Model (DEM) Using Transform-Based Watermarking. *ISPRS Int. J. Geo-Inf.* **2022**, *11*, 200. https://doi.org/10.3390/ijgi11030200

Academic Editors: Raffaele Albano and Wolfgang Kainz

Received: 5 November 2021
Accepted: 14 February 2022
Published: 16 March 2022

1. Introduction

Open data are a set or multiple of digital data made for free use and are available, reused, utilized, and redistributed by anyone without restrictions from ownership, copyright, or other mechanism control standards, thus respecting the law by citing the source and owner of the data (e.g., intellectual property rights). Open data enable users to contribute to public planning, provide feedback for the service quality of the government, and compare and combine different datasets that can help identify trends, challenges, and inequities in the social and economic sectors. Transparency of public information is a significant characteristic of a democratic country, in which obtaining data and information is a human right.

Geospatial data are used to support national interests (e.g., hydrodynamic modeling to assess the impact of tidal flooding on salt production) [1]. The same data can also be used for tsunami modeling [2], tidal simulation [3], and other purposes. Moreover, geospatial data and information are strategically placed with statistical and financial data for development planning in any country. Geospatial data are related to data and information that show the location and status of an object or event in a particular coordinate system below, on, or above the Earth's surface; thus, these data have unique formats, such as georeferenced data and information, geodata, and geoinformation.

One geospatial data format is GeoTIFF. GeoTIFF is based on the TIFF format with embedded georeferencing information and is widely used in NASA Earth Science data systems. It has TIFF tags, including the following raster metadata, such as spatial extent, projection, datums, cartographic information, ellipsoid coordinate reference system, and resolution in raster format (comprising pixels), mainly as a distribution format for digital elevation model (DEM), data satellite, or aerial photography imagery and digital ortho quadrangle data [4–7]. A DEM represents the Earth's bare ground (bare earth) topographic surface, excluding trees, buildings, and any other surface objects. DEM is also a raster representation of a continuous surface, usually referencing the surface of the Earth that is processed as a Geographic Information System (GIS) layer generated from remotely sensed data collected by satellites, drones, and planes. The accuracy of these data is primarily determined by the resolution (distance between sample points). Other factors affecting accuracy include data type (integer or floating-point) and the actual sampling of the surface during the creation of the original DEM.

Basic geospatial information in the form of satellite images (raster), topographic maps (vector), and the national height matrix or the National Digital Elevation Model (*Seamless DEM dan Batimetri Nasional*—DEMNAS) are the main products of the Geospatial Information Agency of Indonesia (*Badan Informasi Geospasial*—BIG), available in its geoportal [8]. Ownership protection for DEM in GeoTIFF format will be different from that in a triangulated irregular network (TIN), which may only be possible via zero watermarking [9]. The TIN represents a surface as a set of contiguous, non-overlapping triangles, which is a particular DEM case. The simulation results show that the method has good robustness against translation, rotation, scaling, and cropping attacks. The construction of the zero watermarks is emphasized by collecting all the triangles from the original data. The core part of zero watermarking involves the selection of the stable characteristic and the construction of the watermark. A stable characteristic indicates remaining unchanged or only slightly changed regardless of the type and intensity of attacks received by the data. The robustness of zero watermarking mainly originates from this stability. In the proposed method, the relationship of edge lengths is the stable characteristic of the TIN DEM data. However, this finding is different from that of the current study because GeoTIFF was used as the research object. Watermarking is still necessary based on the purpose of the current study. Therefore, the host image is considered a BIG production as long as at least 10% of a watermark can be extracted from the embedded image after the host image is attacked.

The growth of the open geospatial data movement encounters challenges in data protection implementation, followed by the rising threats in intellectual property rights. Thus, upholding geospatial data integrity and preventing illegal copy alteration of data is necessary. Copyright protection using copy prevention methods, copyright ownership, data falsification prevention, illegal duplication, or data piracy is starting to emerge. Therefore, providing security in spatial data with techniques to prevent piracy and falsification simultaneously is necessary. This security must meet the following requirements: (1) it must be invisible in the data, (2) it must be attached to the data (not in the app), (3) the security techniques cannot affect the quality of the data because users with various applications will further process this data, and 4) it must not damaged by any spatial operations, such as cropping, merging, or partial updating.

Watermarking is an ownership protection method [10–17]. Furthermore, this method is sensitive to slight modification, allowing for the easy detection of any manipulation (by data attacking). This research performed tests with multiple scenarios on transform-based watermarking, such as the two-dimensional discrete Fourier transform (2D DFT), discrete cosine transform (2D DCT), and discrete wavelet transform (2D DWT). The DCT, DFT, and DWT algorithms are already widely used in various applications; therefore, many ready-to-use function libraries are available, making it easier for software developers to develop. Interestingly, other algorithms [18,19] can be modified for future use in DEM.

2. Materials

The developed security algorithms shall include the following: algorithms for georeferenced multispectral raster image data (e.g., in GeoTIFF format, 8 bits per band), DEMNAS data where each cell contains 32-bit elevation information (also GeoTIFF format), and vector-structured topographic map data (e.g., in format ESRI-Shape file, SHP). The geometric aspect must also be considered to preserve geospatial information quality because the aforementioned data are for national development mapping purposes in Indonesia. Therefore, the Regulation of Head of the BIG Number 6 of 2018 regarding technical guidelines for base map accuracy [20] in Table 1 is used as a reference, and the accuracy value in each class is obtained through the provisions as shown in Table 2 below.

The base map position error does not exceed the accuracy value with a confidence level of 90%. Therefore, CE90 and LE90 values can be obtained by the formula based on the following standard of the United States National Map Accuracy Standards (The US NMAS): CE90 = 1.5175 × RMSEr and LE90 = 1.6499 × RMSEz, in which RMSEr means root mean square error on the x and y horizontal positions and RMSEz denotes root mean square error on the z vertical position.

The developed security algorithms must meet the demand for ownership protection, that is, all these algorithms must be fast in encryption and decryption: Encryption must be performed in batches for all related data in the data center or conducted while in motion or progress when the user accesses the data, and decryption must be performed "on the fly" for the data encountered. Therefore, all algorithms must be implemented in applications that are proven to run fast. The objective is to test the performance and durability of three watermarking algorithms, namely, the 2D DFT, 2D DCT, and 2D DWT, despite their limited use for spatial data, particularly vector maps [21].

The data used in this research include those from the national digital elevation model (DEMNAS). DEM data are essential for engineering works, such as irrigation planning; roads, bridges, and dams; soil volume calculation; visibility analysis; and telecommunication radio wave propagation analysis. Therefore, DEM requires high accuracy [21]. Nonetheless, the obtained accuracy of DEM should not be significantly reduced due to the watermarking process. In the data center, DEM data are stored in tiles with an identity in the form of a map sheet number, from which the latitude–longitude coordinates of the data corners can be immediately known. The spatial resolution of DEMNAS is 0.27 arcsecond using the EGM2008 vertical datum, and the data format is a 32-bit float GeoTIFF. The GeoTIFF format is used throughout the geospatial data to share geographic image data from satellite imaging systems, aerial photography, scanned maps, DEMs, or geographic analyses. The description of the data is presented in Table 3.

Table 1. Geometric accuracy on the national topographic map of Indonesia.

Scale	Contour Interval (Meters)	Topographic Map Accuration					
		Quality of First Class		Quality of Second Class		Quality of Third Class	
		Circular Error 90% (CE90) of Horizontal in Meters	Linear Error 90% (LE90) of Vertical in Meters	Circular Error 90% (CE90) of Horizontal in Meters	Linear Error 90% (LE90) of Vertical in Meters	Circular Error 90% (CE90) of Horizontal in Meters	Linear Error 90% (LE90) of Vertical in Meters
1:1,000,000	400	300	200	600	300	900	400
1:500,000	200	150	100	300	150	450	200
1:250,000	100	75	50	150	75	225	100
1:100,000	40	30	20	60	30	90	40
1:50,000	20	15	10	30	15	45	20
1:25,000	10	7.5	5	15	7.5	22.5	10
1:10,000	4	3	2	6	3	9	4
1:5000	2	1.5	1	3	1.5	4.5	2
1:2500	1	0.75	0.5	1.5	0.75	2.3	1
1:1000	0,4	0.3	0.2	0.6	0.3	0.9	0.4

Table 2. Geometric accuracy requirements on the national topographic map of Indonesia based on the quality classification.

Accuration	Quality of First Class	Quality of Second Class	Quality of Third Class
Horizontal	0.2 mm × map scale numbers	0.3 mm × map scale numbers	0.5 mm × map scale numbers
Vertical	0.5 × contour interval numbers	1.5 × contour interval numbers of the 1st class	2.5 × contour interval numbers of the 1st class

Table 3. Data Description.

Item	Description	DEMNAS
File name	DEMNAS_xxxx-yyy-v1.0.tif for 1:25k. xxxx-yy shows the RBI map sheet number, and v1.0 indicates the 1.0 version release. DEMNAS_1209-14 (typically undulating to the moderately sloping area—highlands), DEMNAS_1209-42 (typically flat to the undulating area), and DEMNAS_1209-44 (typically flat area—coastal plains) are used.	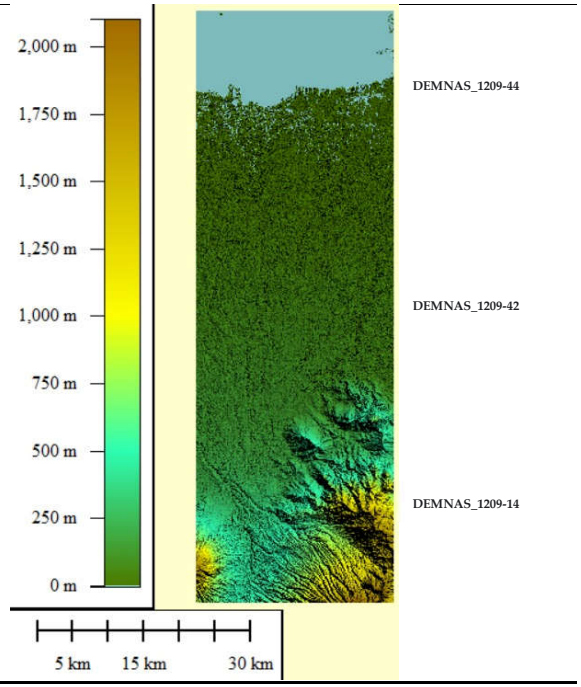
Resolution	0.27 arcsecond	
Datum	EGM2008 vertical datum	
Coordinate system	Geographic	
Format	32-bit float GeoTIFF	
Sources	The National DEM is built from several data sources, including IFSAR data (5 m resolution) and ALOS PALSAR (11.25 m resolution), by adding Masspoint data from stereo plotting results	
Information	DEMNAS data for the area used are compatible for large- to medium-scale mapping (≤1:10,000 to 1:250.000)	

The "CIA triad" (Confidentiality–Integrity–Availability) is a widely used benchmark for evaluating the effectiveness of information system security [22]. This research scope will only measure "integrity" and include the additional "Non-repudiation" parameters to facilitate the purpose of watermarking in geospatial information, in which their creators/ownership should be undeniable. Through the prerequisite, this research method will prove that the proposed solution would be able to hold DEM "data integrity" through copyright (data ownership) assurance and "Non-repudiation" by tagging its identity or disclaimer function to the process.

3. Methods

The development of watermarking provides many choices: visible or invisible and robust (resistant to attacks) or fragile (easily damaged in the presence of an attack). This study decided that watermarking should be made invisible, robust, general, and a frequency-domain-based embedding technique according to various considerations. This watermarking must be invisible because it should not affect the accuracy of the existing data. Data that may later become inaccurate or even lost should be limited. This watermark must also be resistant to "robust" attacks, such as cropping, merging, or partial altering; that is, the watermark can still be recognized, even if it is not intact, despite the presence of attacks. This watermark must also be "general" to facilitate its application to all data. It does not need to be unique where each part obtained by the user is given its watermark, a kind of serial number on banknotes.

Several digital watermarking methods for 3D polygonal models are available. A public watermarking technique for authenticating Constructive solid geometry (CSG) or boundary representation models also exists [23]. CSG is a modeling technique that uses Boolean operations, such as union and intersection, to combine 3D solids, usually for 3D cadastral data visualization. Another technique is the fragile watermarking method, which detects unauthorized alterations of 3D models [16]. A further technique is wavelet transformation watermarking for 3D polygonal models and multiresolution representation of the polygonal model by embedding in the large wavelet coefficient vectors at one or more resolution levels of detail [13]. Another method involves the robust watermarking of arbitrary triangle meshes from multiresolution analysis by disturbing the original vertices based on the scalar function and watermark information [24]. A parameterization of rational linear functions, whose coefficients of the data-embedding algorithm for non-uniform rational B-spline curves and surfaces [25] are also a digital watermarking method. However, these methods do not apply to DEM, a raster with elevation (3D) information. This phenomenon is due to the utilized computer-aided design software, which cannot accept changes to the topology and/or geometry of the model due to existing data-embedding techniques. Their algorithm preserves the shape of its embedding targets (geometry and topology) in CAD applications. CAD models rarely tolerate geometry and/or topology changes introduced by existing data-embedding algorithms. Thus, changes in the topology of geometric primitives will become a problem (e.g., in the case of finite element analysis, in which the preservation of the connectivity of elements is essential). The watermarking technique must protect GeoTIFF data. Xu [26] reconstructed texture images using DWT, which can achieve high classification accuracy, while Huang [7] performed watermarking to process extensive GeoTIFF data directly using Hadoop-based technology. Notably, the watermark may not remove or change the obtained spatial information under GeoTIFF watermarking.

However, the result of the model in the previous research cannot address the demand for ownership protection. Doglioni [27] obtained detail coefficients of DEM and evidence of their variations and values based on 2D DWT of DEMS. Ensuring that attacks cannot quickly destroy the embedded watermarking data on GeoTIFF by performing the following scenarios is necessary: (1) visibility (human visible system and RMSE), (2) calculation of insertion efficacy by multiplying the extracted watermark by the original watermark by 100%, (3) fidelity of peak signal-to-noise ratio (PSNR), (4) data payload, and (5)

robustness by testing on geometric operations, such as cropping/clipping, scaling, re-projection, and others.

The constructed watermarking method is presented in Figure 1. The blue shapes represent an inserted process, while the pink shapes represent extracted process.

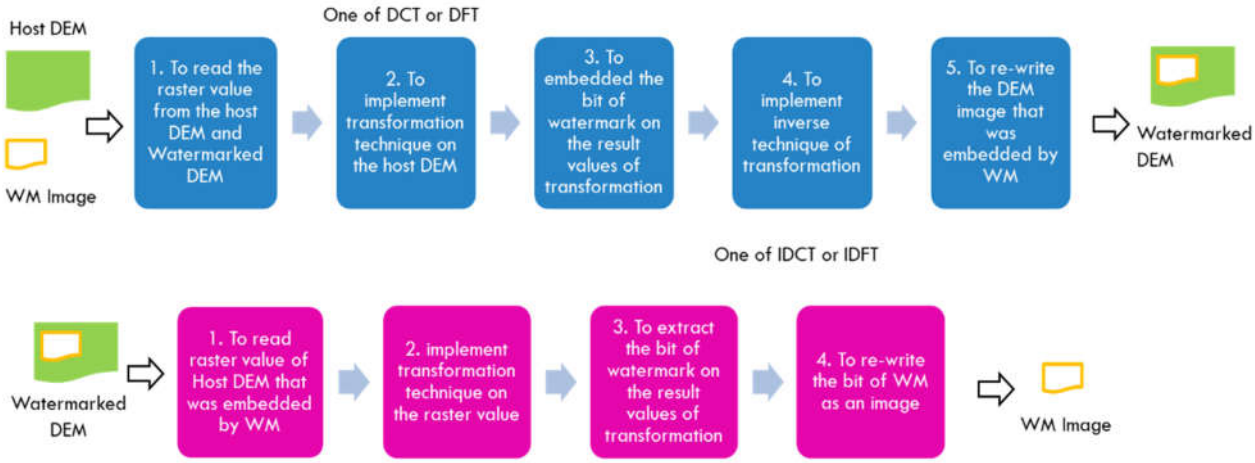

Figure 1. Construction of watermarking technique.

The watermarking technique used further in this research is robust watermarking based on the end of applications. This technique is selected because the embedded watermark will remain on the image despite attacks. Attack types include cropping, scaling, reprojection, filtering, translation, rotation, resizing, and compression. Robust watermarking can serve as a form of copy protection; therefore, the label of the owner can be detected in a suspected copy [16]. The current research focuses on resizing by clipping or cropping to test the robustness aspect.

The following two watermarking methods are most often used: the spatial and frequency domains [28]. Watermarking with a domain frequency scheme has superior robustness and transparency [29]. The frequency domain-based watermark technique is also proven to have a higher level of imperceptibility than the spatial domain technique. The most widely used transformation techniques are DCT, DFT, and DWT. The transformation technique is robust and resistant to low-pass filters, blurring, and sharpening but weak against cropping and scaling attacks. The DWT technique is often applied together with DCT, small capacity, and heavy computing [30,31].

Watermarks should meet the elements of invisibility, resistance to various algorithms, and detectability [28]. The transformed image must be tested for quality. Shrestha et al. [32] tested the compressed image using the MSE, RMSE, PSNR, and correlation coefficient values. A recent review outlines that the most used metrics for watermarked vector map fidelity are RMSE and PSNR, which are both error metrics based on the mean square error. The output of error metrics indicates the precise loss caused by the watermarking process [31]. Our study performed quality testing according to the standards outlined in the Basic Map Accuracy Technical Guidelines [20].

The watermarking application has two primary programs: the insertion process program, which inserts a label image or proprietary label into the protected picture, and the extraction process program, which acts as a label detector embedded in the image. First, the host image is read, and each layer is detached. Each layer will be associated with a proprietary label (image label), converted to binary, and then provided with additional robustness to ensure that the integrity of the watermark image is maintained during an attack and extraction process. The label image matrix is scaled to match the size of the host

picture. The label image should not be larger than the host picture to retain the image quality throughout distribution; thus, each layer of the host and label images is transformed. The label image is then copied into each layer of the modified host image. For extracting and detecting, the host and watermarked images are both inputs to extracting or detecting labels from the watermarked image. Both images are then processed, and the outcome is a label image (ownership label), which is returned to the user.

Practically, the Host DEM file in this experiment is read and then transformed in accordance with the "algorithm" with a watermark image, replaces insignificant values in certain cells, and is then written back to the watermarked DEM file. For extraction, the watermarked DEM file is read, and then certain cells are transformed back with an "algorithm" to read the watermark image (if any). Therefore, this process is watermark blind; that is, it does not require a native DEM host or a native watermark. The "algorithm" has several possible methods: DCT, DFT, and DWT.

The first method is DCT, which transforms the time domain to the frequency domain. DCT employs only real values [33]. It also helps separate the image into sections (or spectral sub-bands) for different purposes regarding the visual quality of the image. Similar to a DFT, DCT converts a signal or image from the spatial to the frequency domain. The watermarking process using DCT is modified from Li [33] as follows: (1) selection of the DEM image to be used (host/original image); (2) defying the watermark logo; and (3) conversion of the previously selected host picture into a DCT domain that is divided into blocks and the computation of the DCT coefficients for each block. If bit 1 is set, then all coefficients become odd numbers; if bit 0 is set, then all coefficients become even values. The remainder of the coefficients are quantized to obtain qualitative inverses, and then (4) a watermark logo is inserted into each selected block. The 2D DCT block calculates the 2D DCT of an image. Suppose $f(x,y)$ is the input image of dimension M-by-N, then the equation for the 2D DCT [34] is:

$$F(m,n) = \frac{2}{\sqrt{MN}} C(m)\ C\ (n) \sum_{x=0}^{M-1} \sum_{y=0}^{N-1} f(x,y)\ cos\ cos\ \frac{(2x+1)mx}{2M}\ cos\ \frac{(2y+1)nx}{2N}, \quad (1)$$

where

$$\mathrm{C}(m) = \mathrm{C}(n) = 1/\sqrt{2} \text{ for } m, n = 0 \text{ and } \mathrm{C}(m), \mathrm{C}(n) = 1 \text{ otherwise.} \quad (2)$$

DWT is an image decomposition at the sub-band frequency of the image. DWT decomposes the signal into a set of orthogonal basis wavelet functions, which differ from sinusoidal basis functions in that they are spatially localized. Similar to the case in Fourier analysis, the DWT is reversible; thus, the original signal can be recovered entirely from its DWT representation. A signal must be run through two DWT filters, specifically high-pass and low pass filters, to evaluate its frequency. The high-pass and low-pass filters are analyzed, with the high pass and low pass filters examining the high and low frequencies, respectively [35–37].

DWT decomposes an image into four wavelet sub-bands: LL, HL, LH, and HH, with LL being a low-frequency sub-band. The process is modified as follows: (1) choosing the DEM image to be used (host/original image); (2) defining the watermark logo; (3) using a single level of DWT, thereby decomposing the host image into LL, HL, LH, and HH; (4) utilizing a single level of DWT and decomposing the host image into LL, HL, LH, and HH, which is the initial step in inserting a watermark into the original image; (5) converting the arrangement of the image into a series of matrices through vectorization; (6) inserting the watermark image into the original image after transforming the original and watermark images with DWT. The approximation coefficient on the original image is added by multiplying the specified key with the watermark approximation coefficient. This process obtains a new approximation coefficient from the original image and (7) displays a watermarked DEM image. The scaling function and expansion coefficients on

DWT can be calculated from the inner product of f˜(t) with φ(t) and ψ(t) or, equivalently, from the inner product of f(t) with the periodized φ˜(t) and ψ˜(t):

$$c\tilde{}_j(k) = \langle f\tilde{}(t), \varphi(t) \rangle = \langle f(t), \varphi\tilde{}(t) \rangle \quad (3)$$

and

$$d\tilde{}_j(k) = \langle f\tilde{}(t), \psi(t) \rangle = \langle f(t), \psi\tilde{}(t) \rangle, \quad (4)$$

where

$$\varphi\tilde{}(t) = \sum_n \varphi(t + Pn) \text{ and } \psi\tilde{}(t) = \sum_n \psi(t + Pn). \quad (5)$$

This can be seen from:

$$\begin{aligned} d\tilde{}j(k) &= \int_{\infty}^{\infty} f\tilde{}(t)\psi(2^j t - k)dt = \sum_n \int_0^P f(t)\psi(2^j(t + Pn) - k)dt \\ &= \int_0^P f(t)\sum_n \psi(2^j(t + Pn) - k)dt \\ d\tilde{}j(k) &= \int_0^P f(t)\psi\tilde{}(2^j t - k)dt, \end{aligned} \quad (6)$$

where the periodized scaled wavelet is:

$$\psi\tilde{}(2^j t - k) = \sum_n \int_0^P \psi(2^j(t + Pn) - k). \quad (7)$$

DFT is used to facilitate conversion from the spatial to the frequency domain, wherein the DFT contained in the host image is resistant to assault after passing through the transformation [38,39]. Li [40] protected the copyright of a color image based on the combination of quaternion discrete Fourier transform and tensor decomposition. Meanwhile, Li [33] used a robust double-encrypted watermarking algorithm based on the fractional Fourier transform and DCT in the invariant wavelet domain. Computing the 2D Fourier transform of X in the current research is equivalent to first computing the 1D transform of each column of X and then taking the 1D transform of each row of the result. X and Y are shifted by 1 in this formula to reflect matrix indices:

$$Y_{p+1,q+1} = \sum_{j=0}^{m-1} \sum_{k=0}^{n-1} \omega_m^{jp} \omega_n^{kq} X_{j+1,k+1}, \quad (8)$$

where ω_m and ω_n are complex roots of unity defined by the following equations:

$$\omega_m = e^{-2\pi i/m} \omega_n = e^{-2\pi i/n}, \quad (9)$$

where i is the imaginary unit, p and j are indices that run from 0 to m–1, and q and k are indices that run from 0 to n − 1.

4. Results

First, the original DEM downloaded from the national geoportal was watermarked with various methods (2D DCT, 2D DWT, and 2D DFT). The color-coding view shows that the inserted DEM is indistinguishable from the original. However, if a raster calculation between the watermarked and original DEMs is conducted, then a difference of no more than 12 cm is found. This difference is still substantially smaller than the DEMNAS's accuracy, which is larger than 1 m, even in the 6 m range on average. Therefore, this difference can be ignored.

The advantage of the GeoTIFF raster is that it has geotransform metadata, which states the Earth coordinates in the form of X and Y of the pixel located in the top left corner of the image. X and Y mean the Earth's coordinates. If under attacks, such as cropping or clipping, then the x and y values are automatically updated. This research utilizes this geotransform by compiling a coordinate conversion algorithm that focuses on the

conversion of the upper x and y on the cropped image to detect changes in the coordinates of the pixel-cropped image. It has the same projections and references as the original image.

First, the 2D DCT watermark insert scheme starts with the area of the Host DEM that is divided into nine sections. Furthermore, each watermarked image will be inserted in the center area of each section. A bit watermark requires 8 × 8 pixels. Therefore, for a watermark image measuring 66 × 66, an insert area of 528 × 528 pixels is required for the cover image (Figure 2).

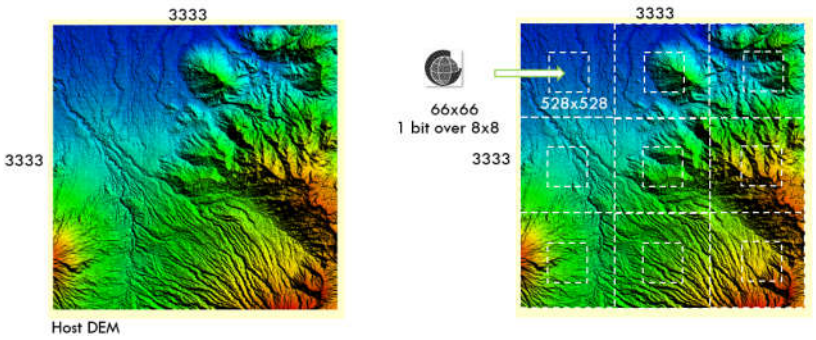

Figure 2. DCT Watermark Insert Scheme.

On the 2D DCT watermark extraction without attack, that is, the watermarked image without any attack, the watermark bits will be extracted directly from each part of the embedding location. The extraction technique is conducted using the same scheme as the insertion technique. Furthermore, watermark bits will be extracted from the center position of each area (Figure 3).

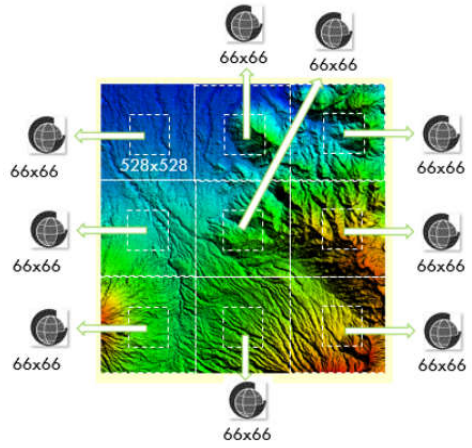

Figure 3. Watermarked DEM.

Watermarked images are likely to experience clipping attacks (Figure 4), as shown in the following illustration. The watermarking technique with DCT can only be extracted if the insertion point has no missing area. For example, for a watermark image measuring 66 × 66 pixels inserted in a 528 × 528 pixel block area on the cover image, the image can only be extracted again if the 528 × 528 block area in the insertion site is not cut off, even if it is only 1 pixel.

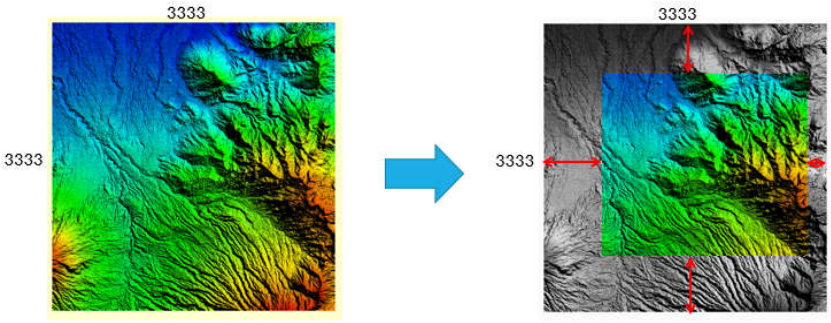

Figure 4. Clipping Attack.

For a clear illustration, Figure 5 below shows that the left image is a watermarked cover image that has not been clipped, while the right image is an image that has undergone clipping. The gray area is the clipped area. The area where the watermark is inserted is divided into nine areas and then provided with an index number as shown in the picture. Therefore, only two watermarks can be re-extracted in this case: watermarks from areas 5 and 6. However, a watermark can be extracted in its entirety, thus sufficiently becoming a marker of copyright ownership.

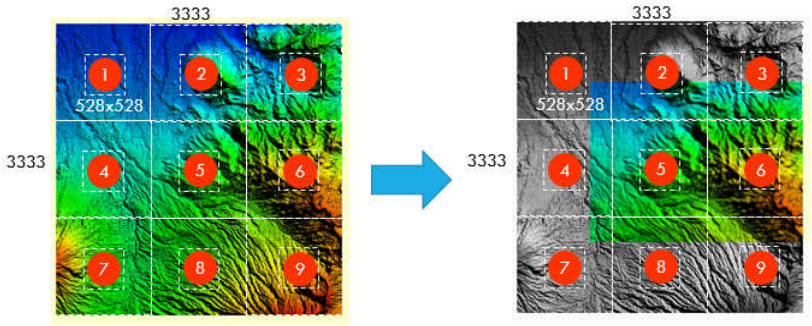

Figure 5. Clear Illustration of Clipping Attack.

A special extraction scheme to countermeasure the clipping attack must be applied. This countermeasure intends to avoid losing the location orientation of the data or the position of the watermark as referred to in the extraction location area during the extraction procedure. The following figure is an illustration of the effects of clipping attacks and techniques to overcome them, which will become the novelty of the current research (Figure 6).

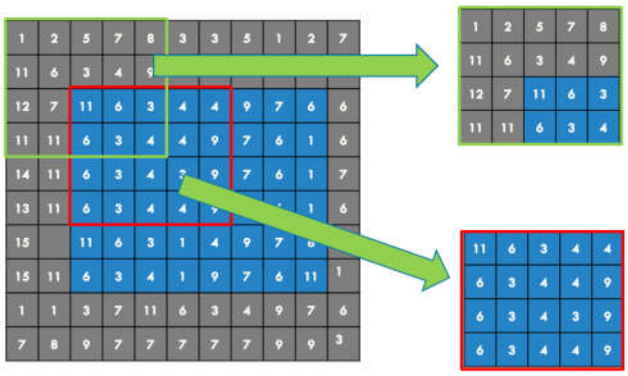

Figure 6. Illustration of Clipping Attack Countermeasures.

The illustrated image shows that the gray area is the clipped image area. Suppose the area with the green border is Microblock-1 (8 × 8), where a WM bit is inserted. The extraction area on the image that has undergone clipping will then be conducted on the red border area, which will be considered as Microblock-1. However, the two macroblocks cannot be declared equal. Therefore, the inserted WM bit will fail (different) when extracted, and extraction failure occurs.

For the extraction solution against clipping attacks, Figure 7 below illustrates that the gray areas are the clipped area, the blue areas are those that are unclipped, and the area with a green border is where the WM bit is inserted. For simplicity, say the area of the insertion of the watermark bit is in the area of 4 × 5 pixels. Furthermore, this illustration indicates that the original watermarked cover is 10 × 11 pixels, the watermarked cover area after clipping is 6 × 8 pixels, and the bit watermarked area is 4 × 5 pixels.

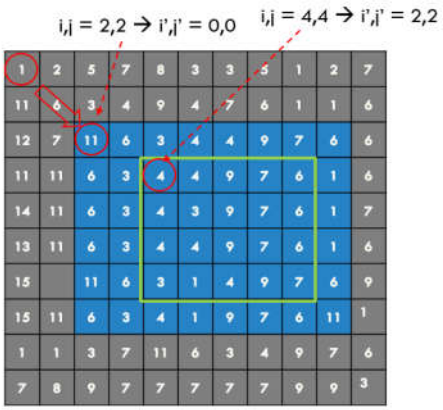

Figure 7. Illustration of extraction solution against clipping attack.

An advantage of GeoTIFF data lies in georeferenced values, one of which is the pair of earth coordinates in the upper left corner (X_{upper}, Y_{upper}) and those in the lower right corner (X_{lower}, Y_{lower}). The georeferenced value will automatically adjust when a GeoTIFF image is clipped. With these properties, the procedure finds the upper left corner point of the block-WM area (green border) with the following steps if the following are met:

- (X_{upper}, Y_{upper}) and (X_{lower}, Y_{lower}) are values of the georeferenced image cover with WM without clipping;
- (X_{upper}', Y_{upper}') and (X_{lower}', Y_{lower}') are the georeferenced image values after a clip (blue area;)

The pixel position of the top left corner (0,0) of the original Host DEM (before clipping) will shift under clipping action. This shift value must be calculated to determine the position of each pixel in the blue area but still use the original coordinate system when the cover has not been clipped. The following steps present the calculation of the shift value:

- Horizontal reference shift (Gx), $Gx = |X_{upper} - X_{upper}'|$;
- Shift in reference vertical direction (Gy), $Gy = |Y_{upper} - Y_{upper}'|$.

Then:

- Nx is the number of pixels horizontally from the original image before clipping;
- Ny is the number of pixels in the vertical direction of the original image before clipping;
- deltaGx = $|X_{upper} - X_{lower}|$;
- deltaGy = $|Y_{upper} - Y_{lower}|$;

so that:

- Horizontal ratio Rx, Rx = Nx/deltaGx;
- Vertical Ratio Ry, Ry = Ny/deltaGy.

The shift of each new pixel position in the x (dx) and y (dy) directions can then be formulated by the following:

1. Shift in x-direction (Dx), Dx = Gx·Rx;
2. Shift in the y (Dy) direction, Dy = Gy·Ry.

Examples of calculations according to the illustration above are given as in the following Table 4.

Table 4. Example of calculations.

Value	Calculation	Attribute
(X_{upper}, Y_{upper})	-	Suppose (100,100)
(X_{lower}, Y_{lower})	-	Suppose (210,200)
(X_{upper}', Y_{upper}')	-	Suppose (120,120)
Nx	-	11
Ny	-	10
deltaGx	$= \lvert X_{upper} - X_{lower} \rvert = \lvert 100–210 \rvert = 110$	110
deltaGy	$= \lvert Y_{upper} - Y_{lower} \rvert = \lvert 100–200 \rvert = 100$	100
Rx	= Nx/deltaGx = 11/110	0.1
Ry	= Ny/deltaGy = 10/100	0.1
Gx	$= \lvert X_{upper} - X_{upper}' \rvert = \lvert 100–120 \rvert = 20$	20
Gy	$= \lvert Y_{upper} - Y_{upper}' \rvert = \lvert 100–120 \rvert = 20$	20
Dx	= Gx·Rx = 20·(0.1) = 2	2
Dy	= Gy·Ry = 20·(0.1) = 2	2

The values of Dx = 2 and Dy = 2 indicate a coordinate shift of 2 pixels to the right and 2 pixels down for each pixel in the new image. Thus, the pixels in position (0,0) or the top left corner of the currently clipped image are actually pixel positions (0 + Dx, 0 + Dy) = (0 + 2, 0 + 2) = (2,2) of the original image before clipping. Another example is the pixel position (2.2), which is the position of the top left corner of the green border area on the clipped image and the position (4,4) in the pixel coordinate system of the original image.

The geotransform function is used to define the upper x and y on the cropped image that has been conducted on this research on an elevation image (single channel) with a size of 3333 × 3333. The image is divided into macroblocks (Figures 4 and 5). The extracted image watermark is only in the area and is not cut off. However, the copyright verification process is generally still thriving. The frequency domain watermark insertion with each macroblock value is transformed into the frequency domain. The image watermark is inserted at each frequency domain value in each macroblock. The inverse transformation is then applied back to the spatial domain value.

The extraction condition for watermarks from the frequency domain indicates that the values in the macroblocks must come from the same area. Figure 8 shows that the white and red borders are the boundaries of the macroblock area during watermark insertion and extraction, respectively. Successfully extracted watermarks will not be lost because the red and white borders are out of sync.

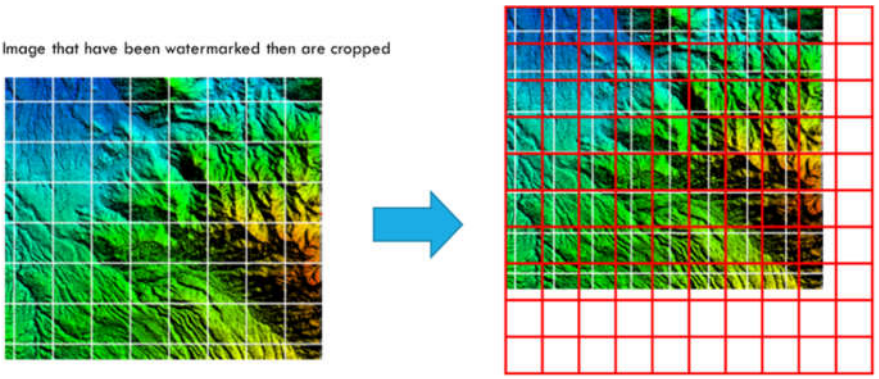

Figure 8. Watermark condition with different macroblocks.

5. Discussion

The impact of cropping on the frequency domain watermark scheme should also be considered. The extraction condition for watermarks from the frequency domain indicates that the values in the macroblocks must come from the same area. Therefore, each macroblock area must have an orientation point of reference or an area marker. The macroblock area will be identified on the basis of the reference orientation when cropping is completed. The watermark is extracted from the macroblock after the macroblock area has been identified. Macroblocks are distributed at specific intervals in this research (Figure 9). The red mark is the marker in the upper left corner of the macroblock area. The marker is positioned in column m-1 and row n-1 from the top left corner, located on the macroblock (m rows, n column). Marker values operate in the spatial domain (for contours, it indicates elevation values). The marker is recognized from its value: for example, the value of the last three decimal digits with a unique form of xxx.xx555. The number 555 is chosen to be in the middle value of three digits behind the comma. Error shifting is observed in the range of 0.00555 m (still allowed in accordance with technical rules).

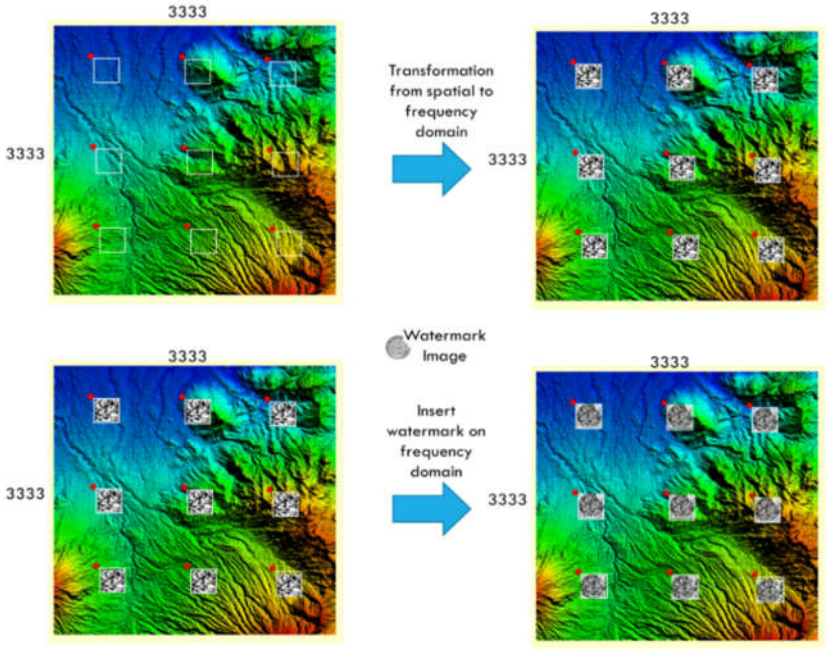

Figure 9. Macroblocks that are distributed at specific intervals on the one scene of GeoTIFF.

First, the steps intended to test the most potential watermark technique on DEMNAS data (Figure 10) are discussed. The DCT watermark technique can retain the watermark bits to be re-extracted in 100% completion (Table 5). In addition, the distortion value of the elevation data with the DCT technique demonstrates the smallest maximum value of 0.1 m compared with 4.5 and 1.1 m for DFT and DWT, respectively. The following five different image watermarks were used in the experiment.

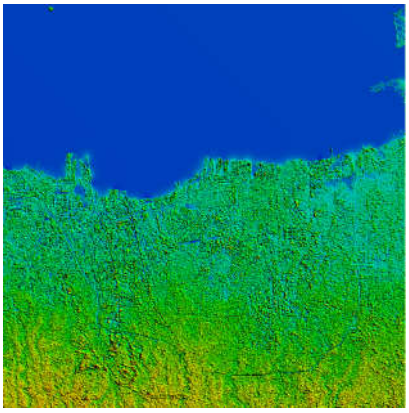

Figure 10. DEMNAS_1209-44_v1.0.tif.

Table 5. BIG's logo used on DCT and DFT.

Nr.	Watermark Image File	Dimension (Pixels)	Image
1	Logo_BIG_Black_33x33.png	33 × 33	
2	Logo_BIG_Black_66x66.png	66 × 66	
3	Logo_BIG_Black_132x132.png	132 × 132	
4	BIG_Black_66x66.png	66 × 66	
5	BIG_White_66x66.png	66 × 66	

Second, the Indonesian National DEM Nasional/DEMNAS) data, namely, DEMNAS_1209-44_v1.0.tif (3333 × 3333 pixels), were employed using the 2D DCT technique. The experimental results indicate that the difference in the dimensions and the shape pattern of the watermark images does not generally affect the value of the evaluation parameter. The experiments prove that the DCT technique can re-extract every watermark image (Table 5) completely (100%), and the results are presented in Tables 6–10 below. Figure 11 shows that the DEM that has been inserted by the watermark in a human visual system has not changed. Figure 11 reveals that the differences in Z value (elevation) between watermarked DEM and Host DEM are less than 12 cm.

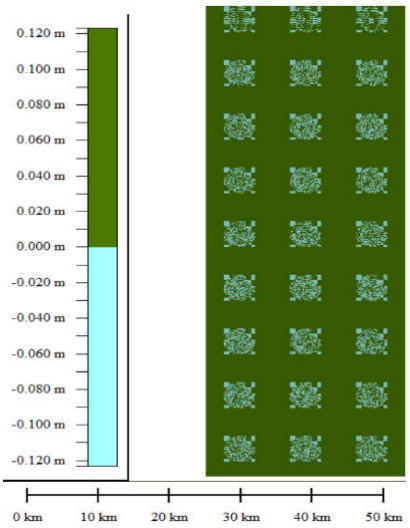

Figure 11. Differences in Z value (elevation) in watermarked DEM and Host DEM.

Table 6. Results of Experiment 1 (DCT technique).

Nr.	Host DEM	Watermark Image	Watermarked DEM	Extraction Results
1	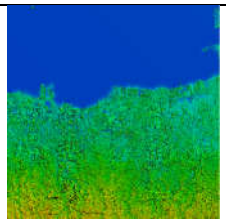 3333 × 3333 pixels	 33 × 33 pixels	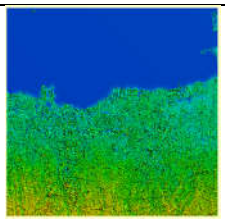 3333 × 3333 pixels	 99 × 99 pixels
2	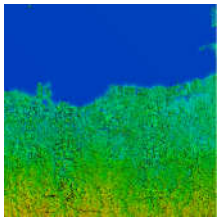 3333 × 3333 pixels	 66 × 66 pixels	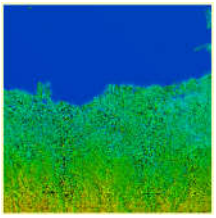 3333 × 3333 pixels	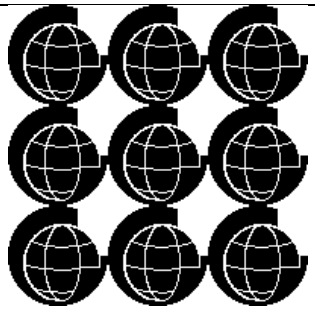 198 × 198 pixels

3	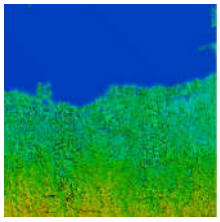 3333 × 3333 pixels	 132 × 132 pixels	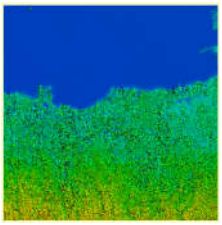 3333 × 3333 pixels	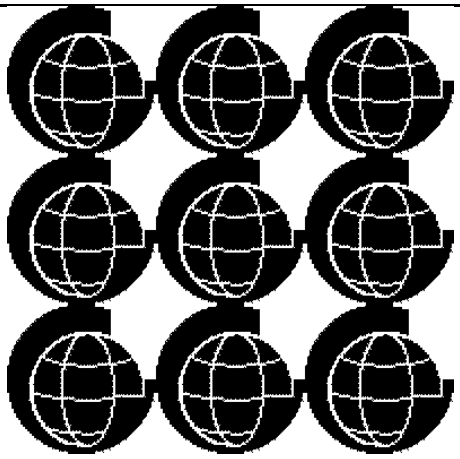 396 × 396 pixels
4	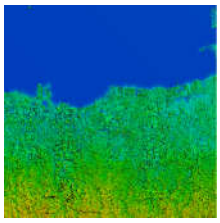 3333 × 3333 pixels	 66 × 66 pixels	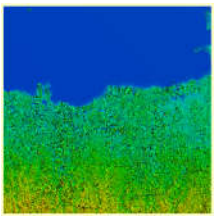 3333 × 3333 pixels	 198 × 198 pixels
5	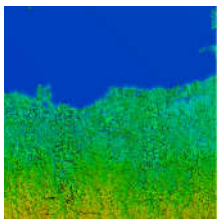 3333 × 3333 pixels	 66 × 66 pixels	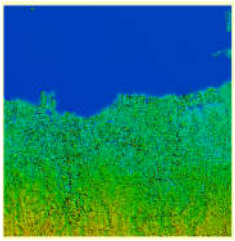 3333 × 3333 pixels	 198 × 198 pixels

Table 7. Experimental results of the evaluation parameter of extracted watermark.

Nr.	Host DEM	Watermarked DEM	Watermark Image	Technique	Extracted Watermark
1	DEMNAS_1209-44_v1.0.tif	DCT_DEMNAS_1209-44_v1.0_berWM_Logo_BIG33.tif	Logo_BIG_Black_33x33.png	DCT	100
2	DEMNAS_1209-44_v1.0.tif	DCT_DEMNAS_1209-44_v1.0_berWM_Logo_BIG66.tif	Logo_BIG_Black_66x66.png	DCT	100
3	DEMNAS_1209-44_v1.0.tif	DCT_DEMNAS_1209-44_v1.0_berWM_Logo_BIG132.tif	Logo_BIG_Black_132x132.png	DCT	100
4	DEMNAS_1209-44_v1.0.tif	DCT_DEMNAS_1209-44_v1.0_berWM66_BIG_Black.tif	BIG_Black_66x66.png	DCT	100
5	DEMNAS_1209-44_v1.0.tif	DCT_DEMNAS_1209-44_v1.0_berWM66_BIG_White.tif	BIG_White_66x66.png	DCT	100
6	DEMNAS_1209-44_v1.0.tif	DFT_DEMNAS_1209-44_v1.0_berWM_Logo_BIG33.tif	Logo_BIG_Black_33x33.png	DFT	84.30
7	DEMNAS_1209-44_v1.0.tif	DFT_DEMNAS_1209-44_v1.0_berWM_Logo_BIG66.tif	Logo_BIG_Black_66x66.png	DFT	85.97
8	DEMNAS_1209-44_v1.0.tif	DFT_DEMNAS_1209-44_v1.0_berWM_Logo_BIG132.tif	Logo_BIG_Black_132x132.png	DFT	86.01
9	DEMNAS_1209-44_v1.0.tif	DFT_DEMNAS_1209-44_v1.0_berWM66_BIG_Black.tif	BIG_Black_66x66.png	DFT	94.21
10	DEMNAS_1209-44_v1.0.tif	DFT_DEMNAS_1209-44_v1.0_berWM66_BIG_White.tif	BIG_White_66x66.png	DFT	90.50
11	DEMNAS_1209-14_v1.0.tif	DEMNAS_1209-14_di_33.tif	Logo_BIG_Black_33x33_14_rec.png	DWT-DCT	100
12	DEMNAS_1209-14_v1.0.tif	DEMNAS_1209-14_di_66.tif	Logo_BIG_Black_66x66_14_rec.png	DWT-DCT	100
13	DEMNAS_1209-14_v1.0.tif	DEMNAS_1209-14_di_132.tif	Logo_BIG_Black_132x132_14_rec.png	DWT-DCT	100
14	DEMNAS_1209-14_v1.0.tif	DEMNAS_1209-14_di_b.tif	BIG_Black_66x66.png	DWT-DCT	100
15	DEMNAS_1209-42_v1.0.tif	DEMNAS_1209-42_di_33.tif	Logo_BIG_Black_33x33_42_rec.png	DWT-DCT	100
16	DEMNAS_1209-42_v1.0.tif	DEMNAS_1209-42_di_66.tif	Logo_BIG_Black_66x66_42_rec.png	DWT-DCT	100
17	DEMNAS_1209-42_v1.0.tif	DEMNAS_1209-42_di_132.tif	Logo_BIG_Black_132x132_42_rec.png	DWT-DCT	100
18	DEMNAS_1209-42_v1.0.tif	DEMNAS_1209-42_di_b.tif	BIG_Black_66x66.png	DWT-DCT	100
19	DEMNAS_1209-44_v1.0.tif	DEMNAS_1209-44_di_33.tif	Logo_BIG_Black_33x33_14_rec.png	DWT-DCT	100
20	DEMNAS_1209-44_v1.0.tif	DEMNAS_1209-44_di_66.tif	Logo_BIG_Black_66x66_14_rec.png	DWT-DCT	100
21	DEMNAS_1209-44_v1.0.tif	DEMNAS_1209-44_di_132.tif	Logo_BIG_Black_132x132_14_rec.png	DWT-DCT	100
22	DEMNAS_1209-44_v1.0.tif	DEMNAS_1209-44_di_b.tif	BIG_Black_66x66.png	DWT-DCT	100

Table 8. Experimental results of the evaluation parameter of Max Delta.

Nr	Host DEM	Watermarked DEM	Watermark Image	Technique	Max Delta (m)
1	DEMNAS_1209-44_v1.0.tif	DCT_DEMNAS_1209-44_v1.0_berWM_Logo_BIG33.tif	Logo_BIG_Black_33x33.png	DCT	0.021
2	DEMNAS_1209-44_v1.0.tif	DCT_DEMNAS_1209-44_v1.0_berWM_Logo_BIG66.tif	Logo_BIG_Black_66x66.png	DCT	0.021
3	DEMNAS_1209-44_v1.0.tif	DCT_DEMNAS_1209-44_v1.0_berWM_Logo_BIG132.tif	Logo_BIG_Black_132x132.png	DCT	0.022
4	DEMNAS_1209-44_v1.0.tif	DCT_DEMNAS_1209-44_v1.0_berWM66_BIG_Black.tif	BIG_Black_66x66.png	DCT	0.023
5	DEMNAS_1209-44_v1.0.tif	DCT_DEMNAS_1209-44_v1.0_berWM66_BIG_White.tif	BIG_White_66x66.png	DCT	0.023
6	DEMNAS_1209-44_v1.0.tif	DFT_DEMNAS_1209-44_v1.0_berWM_Logo_BIG33.tif	Logo_BIG_Black_33x33.png	DFT	4.874
7	DEMNAS_1209-44_v1.0.tif	DFT_DEMNAS_1209-44_v1.0_berWM_Logo_BIG66.tif	Logo_BIG_Black_66x66.png	DFT	4.578
8	DEMNAS_1209-44_v1.0.tif	DFT_DEMNAS_1209-44_v1.0_berWM_Logo_BIG132.tif	Logo_BIG_Black_132x132.png	DFT	4.713
9	DEMNAS_1209-44_v1.0.tif	DFT_DEMNAS_1209-44_v1.0_berWM66_BIG_Black.tif	BIG_Black_66x66.png	DFT	5.643
10	DEMNAS_1209-44_v1.0.tif	DFT_DEMNAS_1209-44_v1.0_berWM66_BIG_White.tif	BIG_White_66x66.png	DFT	2.064
11	DEMNAS_1209-14_v1.0.tif	DEMNAS_1209-14_di_33.tif	Logo_BIG_Black_33x33_14_rec.png	DWT-DCT	1.139
12	DEMNAS_1209-14_v1.0.tif	DEMNAS_1209-14_di_66.tif	Logo_BIG_Black_66x66_14_rec.png	DWT-DCT	1.160
13	DEMNAS_1209-14_v1.0.tif	DEMNAS_1209-14_di_132.tif	Logo_BIG_Black_132x132_14_rec.png	DWT-DCT	1.157
14	DEMNAS_1209-14_v1.0.tif	DEMNAS_1209-14_di_b.tif	BIG_Black_66x66.png	DWT-DCT	1.121
15	DEMNAS_1209-42_v1.0.tif	DEMNAS_1209-42_di_33.tif	Logo_BIG_Black_33x33_42_rec.png	DWT-DCT	1.102
16	DEMNAS_1209-42_v1.0.tif	DEMNAS_1209-42_di_66.tif	Logo_BIG_Black_66x66_42_rec.png	DWT-DCT	1.110
17	DEMNAS_1209-42_v1.0.tif	DEMNAS_1209-42_di_132.tif	Logo_BIG_Black_132x132_42_rec.png	DWT-DCT	1.115
18	DEMNAS_1209-42_v1.0.tif	DEMNAS_1209-42_di_b.tif	BIG_Black_66x66.png	DWT-DCT	1.101
19	DEMNAS_1209-44_v1.0.tif	DEMNAS_1209-44_di_33.tif	Logo_BIG_Black_33x33_14_rec.png	DWT-DCT	1.088
20	DEMNAS_1209-44_v1.0.tif	DEMNAS_1209-44_di_66.tif	Logo_BIG_Black_66x66_14_rec.png	DWT-DCT	1.096
21	DEMNAS_1209-44_v1.0.tif	DEMNAS_1209-44_di_132.tif	Logo_BIG_Black_132x132_14_rec.png	DWT-DCT	1.117
22	DEMNAS_1209-44_v1.0.tif	DEMNAS_1209-44_di_b.tif	BIG_Black_66x66.png	DWT-DCT	1.092

Table 9. Experimental results of the evaluation parameter of PSNR.

Nr.	Host DEM	Watermarked DEM	Watermark Image	Technique	PSNR
1	DEMNAS_1209-44_v1.0.tif	DCT_DEMNAS_1209-44_v1.0_berWM_Logo_BIG33.tif	Logo_BIG_Black_33x33.png	DCT	93.514
2	DEMNAS_1209-44_v1.0.tif	DCT_DEMNAS_1209-44_v1.0_berWM_Logo_BIG66.tif	Logo_BIG_Black_66x66.png	DCT	87.601
3	DEMNAS_1209-44_v1.0.tif	DCT_DEMNAS_1209-44_v1.0_berWM_Logo_BIG132.tif	Logo_BIG_Black_132x132.png	DCT	81.507
4	DEMNAS_1209-44_v1.0.tif	DCT_DEMNAS_1209-44_v1.0_berWM66_BIG_Black.tif	BIG_Black_66x66.png	DCT	91.452
5	DEMNAS_1209-44_v1.0.tif	DCT_DEMNAS_1209-44_v1.0_berWM66_BIG_White.tif	BIG_White_66x66.png	DCT	83.814
6	DEMNAS_1209-44_v1.0.tif	DFT_DEMNAS_1209-44_v1.0_berWM_Logo_BIG33.tif	Logo_BIG_Black_33x33.png	DFT	80.772
7	DEMNAS_1209-44_v1.0.tif	DFT_DEMNAS_1209-44_v1.0_berWM_Logo_BIG66.tif	Logo_BIG_Black_66x66.png	DFT	80.320
8	DEMNAS_1209-44_v1.0.tif	DFT_DEMNAS_1209-44_v1.0_berWM_Logo_BIG132.tif	Logo_BIG_Black_132x132.png	DFT	80.427
9	DEMNAS_1209-44_v1.0.tif	DFT_DEMNAS_1209-44_v1.0_berWM66_BIG_Black.tif	BIG_Black_66x66.png	DFT	79.688
10	DEMNAS_1209-44_v1.0.tif	DFT_DEMNAS_1209-44_v1.0_berWM66_BIG_White.tif	BIG_White_66x66.png	DFT	82.604
11	DEMNAS_1209-14_v1.0.tif	DEMNAS_1209-14_di_33.tif	Logo_BIG_Black_33x33_14_rec.png	DWT-DCT	91.474
12	DEMNAS_1209-14_v1.0.tif	DEMNAS_1209-14_di_66.tif	Logo_BIG_Black_66x66_14_rec.png	DWT-DCT	84.772
13	DEMNAS_1209-14_v1.0.tif	DEMNAS_1209-14_di_132.tif	Logo_BIG_Black_132x132_14_rec.png	DWT-DCT	79.039
14	DEMNAS_1209-14_v1.0.tif	DEMNAS_1209-14_di_b.tif	BIG_Black_66x66.png	DWT-DCT	88.675
15	DEMNAS_1209-42_v1.0.tif	DEMNAS_1209-42_di_33.tif	Logo_BIG_Black_33x33_42_rec.png	DWT-DCT	77.585
16	DEMNAS_1209-42_v1.0.tif	DEMNAS_1209-42_di_66.tif	Logo_BIG_Black_66x66_42_rec.png	DWT-DCT	70.887
17	DEMNAS_1209-42_v1.0.tif	DEMNAS_1209-42_di_132.tif	Logo_BIG_Black_132x132_42_rec.png	DWT-DCT	65.154
18	DEMNAS_1209-42_v1.0.tif	DEMNAS_1209-42_di_b.tif	BIG_Black_66x66.png	DWT-DCT	74.789
19	DEMNAS_1209-44_v1.0.tif	DEMNAS_1209-44_di_33.tif	Logo_BIG_Black_33x33_14_rec.png	DWT-DCT	59.594
20	DEMNAS_1209-44_v1.0.tif	DEMNAS_1209-44_di_66.tif	Logo_BIG_Black_66x66_14_rec.png	DWT-DCT	52.897
21	DEMNAS_1209-44_v1.0.tif	DEMNAS_1209-44_di_132.tif	Logo_BIG_Black_132x132_14_rec.png	DWT-DCT	47.163
22	DEMNAS_1209-44_v1.0.tif	DEMNAS_1209-44_di_b.tif	BIG_Black_66x66.png	DWT-DCT	56.800

Table 10. Experimental results of the evaluation parameter of RMSE.

Nr.	Host DEM	Watermarked DEM	Watermark Image	Technique	RMSE
1	DEMNAS_1209-44_v1.0.tif	DCT_DEMNAS_1209-44_v1.0_berWM_Logo_BIG33.tif	Logo_BIG_Black_33x33.png	DCT	0.001129
2	DEMNAS_1209-44_v1.0.tif	DCT_DEMNAS_1209-44_v1.0_berWM_Logo_BIG66.tif	Logo_BIG_Black_66x66.png	DCT	0.002232
3	DEMNAS_1209-44_v1.0.tif	DCT_DEMNAS_1209-44_v1.0_berWM_Logo_BIG132.tif	Logo_BIG_Black_132x132.png	DCT	0.004502
4	DEMNAS_1209-44_v1.0.tif	DCT_DEMNAS_1209-44_v1.0_berWM66_BIG_Black.tif	BIG_Black_66x66.png	DCT	0.001432
5	DEMNAS_1209-44_v1.0.tif	DCT_DEMNAS_1209-44_v1.0_berWM66_BIG_White.tif	BIG_White_66x66.png	DCT	0.005342
6	DEMNAS_1209-44_v1.0.tif	DFT_DEMNAS_1209-44_v1.0_berWM_Logo_BIG33.tif	Logo_BIG_Black_33x33.png	DFT	0.004900
7	DEMNAS_1209-44_v1.0.tif	DFT_DEMNAS_1209-44_v1.0_berWM_Logo_BIG66.tif	Logo_BIG_Black_66x66.png	DFT	0.005162
8	DEMNAS_1209-44_v1.0.tif	DFT_DEMNAS_1209-44_v1.0_berWM_Logo_BIG132.tif	Logo_BIG_Black_132x132.png	DFT	0.005099
9	DEMNAS_1209-44_v1.0.tif	DFT_DEMNAS_1209-44_v1.0_berWM66_BIG_Black.tif	BIG_Black_66x66.png	DFT	0.005552
10	DEMNAS_1209-44_v1.0.tif	DFT_DEMNAS_1209-44_v1.0_berWM66_BIG_White.tif	BIG_White_66x66.png	DFT	0.003968
11	DEMNAS_1209-14_v1.0.tif	DEMNAS_1209-14_di_33.tif	Logo_BIG_Black_33x33_14_rec.png	DWT-DCT	0.003147
12	DEMNAS_1209-14_v1.0.tif	DEMNAS_1209-14_di_66.tif	Logo_BIG_Black_66x66_14_rec.png	DWT-DCT	0.014728
13	DEMNAS_1209-14_v1.0.tif	DEMNAS_1209-14_di_132.tif	Logo_BIG_Black_132x132_14_rec.png	DWT-DCT	0.055136
14	DEMNAS_1209-14_v1.0.tif	DEMNAS_1209-14_di_b.tif	BIG_Black_66x66_14.png	DWT-DCT	0.005996
15	DEMNAS_1209-42_v1.0.tif	DEMNAS_1209-42_di_33.tif	Logo_BIG_Black_33x33_42_rec.png	DWT-DCT	0.003149
16	DEMNAS_1209-42_v1.0.tif	DEMNAS_1209-42_di_66.tif	Logo_BIG_Black_66x66_42_rec.png	DWT-DCT	0.014726
17	DEMNAS_1209-42_v1.0.tif	DEMNAS_1209-42_di_132.tif	Logo_BIG_Black_132x132_42_rec.png	DWT-DCT	0.055136
18	DEMNAS_1209-42_v1.0.tif	DEMNAS_1209-42_di_b.tif	BIG_Black_66x66_42.png	DWT-DCT	0.005997
19	DEMNAS_1209-44_v1.0.tif	DEMNAS_1209-44_di_33.tif	Logo_BIG_Black_33x33_44_rec.png	DWT-DCT	0.003148
20	DEMNAS_1209-44_v1.0.tif	DEMNAS_1209-44_di_66.tif	Logo_BIG_Black_66x66_44_rec.png	DWT-DCT	0.014722
21	DEMNAS_1209-44_v1.0.tif	DEMNAS_1209-44_di_132.tif	Logo_BIG_Black_132x132_44_rec.png	DWT-DCT	0.055127
22	DEMNAS_1209-44_v1.0.tif	DEMNAS_1209-44_di_b.tif	BIG_Black_66x66_44.png	DWT-DCT	0.005993

Next, the experiment was continued to test the watermarking technique with 2D DFT. The Indonesian National DEM Nasional/DEMNAS) data, namely, DEMNAS_1209-44_v1.0.tif (3333 × 3333 pixels), are still employed using the 2D DFT technique. The watermark extraction value is not at 100%, and the distortion to the elevation value is also large, some reaching 5643 m. The displayed watermarked data by the global mapper facilitate easy visualization. The visualization representation of the elevation value of the watermarked data is relatively brighter than the original cover elevation data. The maximum value of the slightest distortion in this DFT technique is when a watermarked image is used with the majority of bits "1" (predominantly white). The max distortion value is 2.064 m in this scenario. In line with these results, visually covered images with watermarks also tend to have elevation color visualizations that are remarkably similar to the original. The extraction of watermarked images with DFT reaches the highest level of 90.50% under the aforementioned scenario. The results are presented in Tables 7–11.

Table 11. Results of Experiment 2 (2D DFT technique).

Nr.	Host DEM	Watermark Image	Watermarked DEM	Extraction Results
1	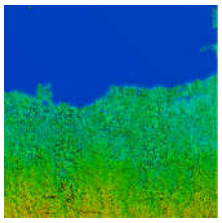 3333 × 3333 pixels	 33 × 33 pixels	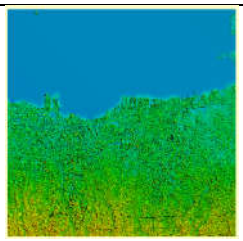 3333 × 3333 pixels	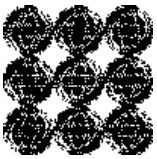 99 × 99 pixels
2	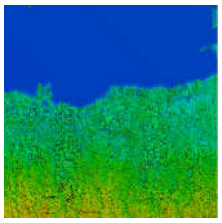 3333 × 3333 pixels	 66 × 66 pixels	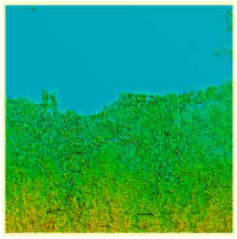 3333 × 3333 pixels	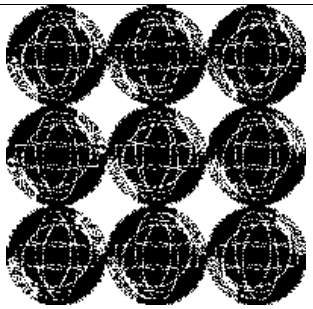 198 × 198 pixels
3	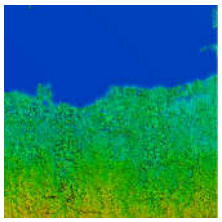 3333 × 3333 pixels	 132 × 132 pixels	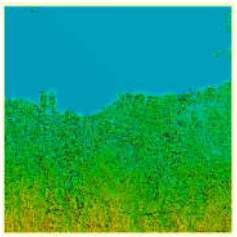 3333 × 3333 pixels	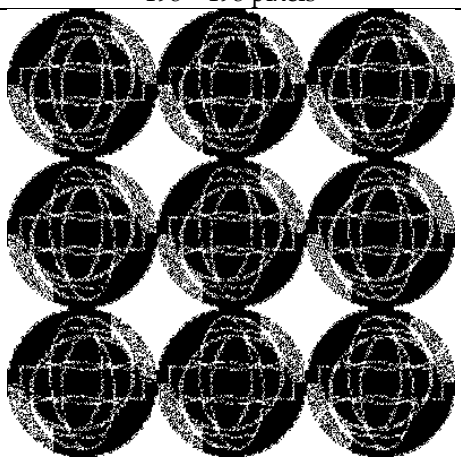 396 × 396 pixels

4	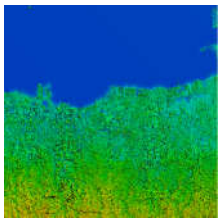 3333 × 3333 pixels	 66 × 66 pixels	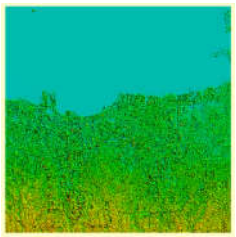 3333 × 3333 pixels	 198 × 198 pixels
5	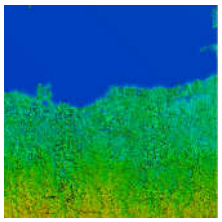 3333 × 3333 pixels	 66 × 66 pixels	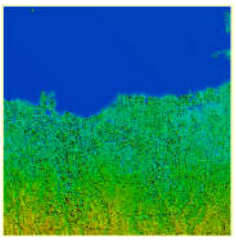 3333 × 3333 pixels	 198 × 198 pixels

Finally, the experiment was continued to test the watermarking technique under combined 2D DCT and DWT. The results on PSNR show that the combination of DWT and DCT is quite good due to its equal application on all image areas. However, RMSE shows that this combination (0.003147) is insufficiently strong compared with DCT (0.001129). Four different watermark images were used in the experiment (Table 12). Therefore, the experimental results of the evaluation parameter of extracted watermark Max Delta (in meters), PSNR, and RMSE are presented in Tables 7–10.

Table 12. BIG's logo used on the DWT and DCT combination.

Nr.	Watermark Image File	Dimension (Pixels)	Image	Extraction Results
1	Logo_BIG_Black_66x66_14_rec.png	66 × 66		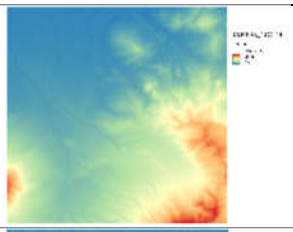
2	Logo_BIG_Black_66x66_42_rec.png	66 × 66		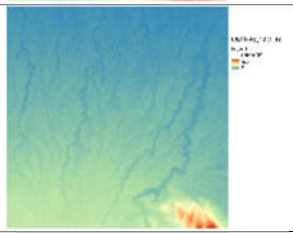
3	Logo_BIG_Black_66x66_44_rec.png	66 × 66		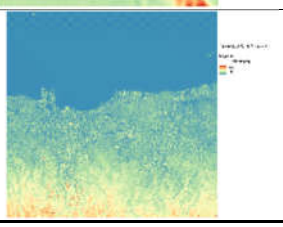

Nr.	Watermark Image File	Dimension (Pixels)	Image	Extraction Results
4	BIG_Black_66x66_44_rec	66 × 66		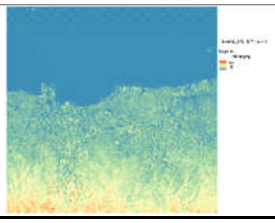

The colored DEM data are reread with the description module to find the BIG logo. The results are presented in Figures 12–14. The 2D DFT method cannot reproduce a perfect logo. The subsequent analysis found that the numbers of Max Delta, PSNR, and RMSE and the percentages of logo integrity (extracted watermark) were different between the 2D DCT, 2D DWT, and 2D DFT methods in the three different DEM areas.

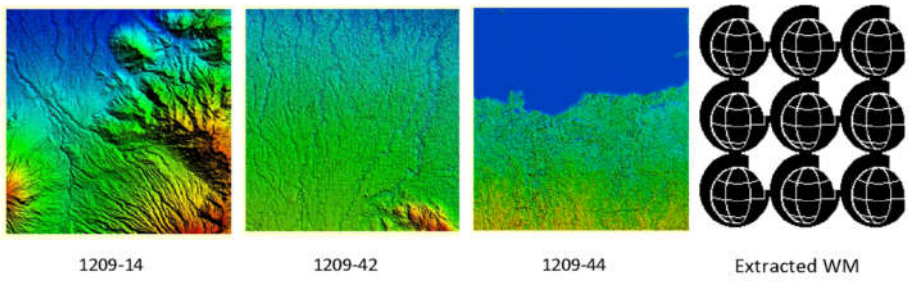

Figure 12. Watermarking results using the 2D DCT algorithm; 100% watermark image extracted with 2D DCT applies equally to all image areas.

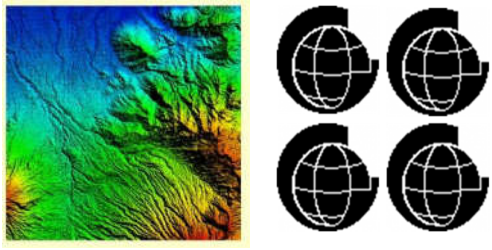

Figure 13. Results of watermarking using a combination of 2D DWT and 2D DCT algorithms; 100% watermark image extraction was realized with 2D DWT and 2D DCT. However, this extraction is not superior to that of DCT only because the distortion to the elevation value is quite large; thus, some extractions reaching 1160 m apply equally to all image areas.

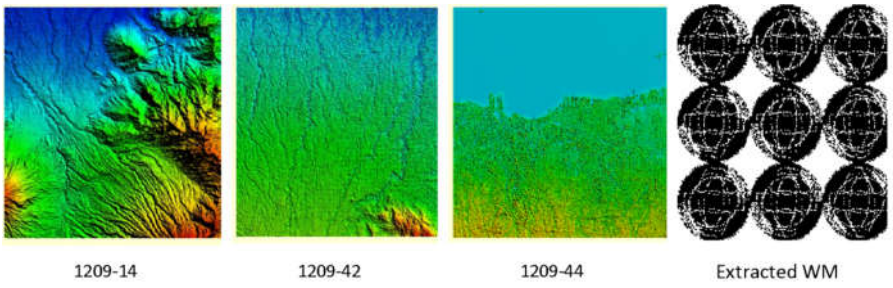

Figure 14. Results of watermarking using the 2D DFT algorithm. The best watermark image that can be extracted with DFT is 94.21%, which is applied on the DEMNAS 1209-44.

6. Conclusions

This experiment shows that DCT, DWT, and FFT techniques have successfully inserted the BIG logo as a watermark on DEM files in a 32-bit GeoTIFF format taken from DEMNAS. DCT technique is better than DWT and FFT. Changes in the contents of areas where the watermark inserted are less than 12 cm. These changes are not visually recognizable unless under comparison with the original DEM file. This technique is ensured to resist attacks as attempted in cropping. Only one of the nine watermarks was detected, but the cropped watermarked DEM was still recognized as DEM data published by BIG. The proposed DCT technique is expected to be an alternative in watermarking techniques for DEM image data types in the mapping field. With a 100% extraction result, no missing bits or errors were observed in the watermark image. The extracted watermark could be identified in visualization and digital computing according to the aforementioned result. This concept is beneficial if the DEM map is disseminated and modified by other parties. The embedded watermark is also adequately tested for the robustness of the cropping technique; thus, it can be proof of legal copyright protection.

Author Contributions: Fahmi Amhar, Endang Purnama Giri, Shelvie Nidya Neyman, Danang Jaya, Anggrahito Anggrahito, and Dadan Ramdani prepared the algorithm and identified DEM characteristics. Florence Elfriede Sinthauli Silalahi, Murdaningsih Murdaningsih, and Sandi Adhitya Kolopaking prepared data samples and related meetings as well as the contact person from stakeholders who provided insights. Fahmi Amhar, Florence Elfriede Sinthauli Silalahi, Dewayany Sutrisno, Tia Rizka Nuzula Rachma, and Sandi Adhitya Kolopaking prepared the references and the first manuscript. Fahmi Amhar, Endang Purnama Giri, Dadan Ramdani, and Anggrahito Anggrahito supervised all the algorithms and performed attack processes to the watermark with necessary modifications. Fahmi Amhar, Endang Purnama Giri, and Florence Elfriede Sinthauli Silalahi wrote the primary section of the paper. All authors have read and agreed to the published version of the manuscript.

Funding: This work was supported by the Geospatial Information Agency of Indonesia (*Badan Informasi Geospasial*) thru DIPA 2021 (3539.EAI.003.054.521219). The study's funders had no role in data analysis and processing, data interpretation, or writing of the report.

Institutional Review Board Statement: Not applicable.

Informed Consent Statement: Not applicable.

Data Availability Statement: DEMNAS can be freely accessed on https://tanahair.indonesia.go.id/demnas/#/. The DEMNAS that we used was accessed on 1 February 2021. Source code can be given case by case as per all author permission.

Acknowledgments: We thank our colleagues from the Center for Research, Public Relations, and Cooperation; the Center for Management and Dissemination of geospatial information; and the Center for Geodetic Control Network and Geodynamics of The Geospatial Information Agency of Indonesia. We are also grateful to the Center for Research and Development of Cyber and Crypto Security Technology—The National Cyber and Crypto Agency; Ian Josef and Yudistira Asnar from the School of Electrical Engineering and Informatics—The Bandung Institute of Technology; and Yohan Suryanto from the Department of Electrical Engineering—the University of Indonesia, who provided DEMNAS data, related documents and insights, and expert inputs that remarkably assisted the research. However, they may not agree with all the interpretations/conclusions of this paper.

Conflicts of Interest: The authors declare that they have no competing interests.

References

1. Nirwansyah, A.W.; Braun, B. Mapping Impact of Tidal Flooding on Solar Salt Farming in Northern Java using a Hydrodynamic Model. *ISPRS Int. J. Geo-Inf.* **2019**, *8*, 451. https://doi.org/10.3390/ijgi8100451.
2. Cummins, P.R.; Pranantyo, I.R.; Pownall, J.M.; Griffin, J.D.; Meilano, I.; Zhao, S. Earthquakes and tsunamis caused by low-angle normal faulting in the Banda Sea, Indonesia. *Nat. Geosci.* **2020**, *13*, 312–318. https://doi.org/10.1038/s41561-020-0545-x.
3. Nuraghnia, A.; Windupranata, W.; Hakim, A.R.; Nusantara, C.A.D.S. Poerbandono Modeling of tide in the Java sea coastal area between Jakarta and Cirebon, Indonesia: Bathymetric data source and sensitivity tests due to bottom roughness and

boundary condition. *IOP Conf. Ser. Earth Environ. Sci.* **2021**, *777*, 012034. https://doi.org/10.1088/1755-1315/777/1/012034.
4. Wasster, L.; Holdgraf, C.; Morrissey, M. About the Geotiff (.tif) Raster File Format: Raster Data in Python. *Earth Data Sci.-Earth Lab.* August 19, 2021. https://www.earthdatascience.org/courses/use-data-open-source-python/intro-raster-data-python/fundamentals-raster-data/intro-to-the-geotiff-file-format/ (accessed on 24 January 2022).
5. NASA. GeoTIFF. *Earth Data*; NASA: Washington, DC, USA, 2021.
6. Mahammad, S.S.; Ramakrishnan, R. GeoTIFF-A standard image file format for GIS applications. In Proceedings of the Map India Conference 2003: Image Processing & Interpretation, Hyderabad, India, 17–20 December 2003.
7. Huang, F.; Zhao, H.; Li, B.; Lv, Z. Watermarking Massive Remote Sensor Images in Parallel. In Proceedings of the 2010 International Conference on Computational Intelligence and Software Engineering, Wuhan, China, 10–12 December 2010; pp. 1–4.
8. Amhar, F. The problematics of Indonesian geoportal and its future strategies. In Proceedings of the 39th Asian Conference on Remote Sensing, Kuala Lumpur, Malaysia, 15–19 October 2019; pp. 1868–1877.
9. Zhou, Q.; Zhu, C.; Ren, N. Zero Watermarking for the TIN DEM Data Based on the Edge Length. *ISPRS Int. J. Geo-Inf.* **2021**, *10*, 559. https://doi.org/10.3390/ijgi10080559.
10. AbouEl-Seoud, S.; Abu Rumman, N.; Taj-Eddin, I.A.T.F.; Khatatneh, K.F.; Gütl, C. Robust Digital Watermarking for Compressed 3D Models based on Polygonal Representation. *Int. J. Comput. Appl.* **2013**, *61*, 1–14. https://doi.org/10.5120/9913-3909.
11. Bors, A.G.; Pitas, I. Image watermarking using DCT domain constraints. In Proceedings of the 3rd IEEE International Conference on Image Processing, Lausanne, Switzerland, 19 September 1996; pp. 231–234.
12. Cho, J.-W.; Prost, R.; Jung, H.-Y. An Oblivious Watermarking for 3-D Polygonal Meshes Using Distribution of Vertex Norms. *IEEE Trans. Signal Process.* **2007**, *55*, 142–155. https://doi.org/10.1109/TSP.2006.882111.
13. Kanai, S.; Date, H.; Kishinami, T. Digital Watermarking for 3D Polygons using Multiresolution Wavelet Decomposition. In Proceedings of the Sixth IFIP WG 5.2/GI Int. Work. Geom. Model. Fundam. Appl. Tokyo, Japan, 1–4 December 1998; pp. 296–307.
14. Li, L.; Zhang, D.; Pan, Z.; Shi, J.; Zhou, K.; Ye, K. Watermarking 3D mesh by spherical parameterization. *Comput. Graph.* **2004**, *28*, 981–989. https://doi.org/10.1016/j.cag.2004.08.002.
15. Ohbuchi, R.; Masuda, H.; Aono, M. Watermarking three-dimensional polygonal models through geometric and topological modifications. *IEEE J. Sel. Areas Commun.* **1998**, *16*, 551–560. https://doi.org/10.1109/49.668977.
16. Yeo, B.-L.; Yeung, M.M. Watermarking 3D objects for verification. *IEEE Comput. Graph. Appl.* **1999**, *19*, 36–45. https://doi.org/10.1109/38.736467.
17. Yin, K.; Pan, Z.; Shi, J.; Zhang, D. Robust mesh watermarking based on multiresolution processing. *Comput. Graph.* **2001**, *25*, 409–420. https://doi.org/10.1016/S0097-8493(01)00065-6.
18. Yamni, M.; Daoui, A.; El, O.; Karmouni, H.; Sayyouri, M.; Qjidaa, H.; Flusser, J. Fractional Charlier moments for image reconstruction and image watermarking. *Signal Processing* **2020**, *171*, 107509. https://doi.org/10.1016/j.sigpro.2020.107509.
19. Tsougenis, E.D.; Papakostas, G.A.; Koulouriotis, D.E.; Tourassis, V.D. The Journal of Systems and Software Performance evaluation of moment-based watermarking methods : A review. *J. Syst. Softw.* **2012**, *85*, 1864–1884. https://doi.org/10.1016/j.jss.2012.02.045.
20. BIG. *Regulation of Head of the Geospatial Information Agency (Badan Informasi Geospasial) Number 6 of 2018 about the amendment to the Regulation of Head of the Geospatial Information Agency of Number 15 of 2014 for Technical Guidelines for Accuracy of Base Map*; Indonesia, 2018. Available online: https://jdihn.go.id/files/217/27330968 (accessed on 10 February 2022).
21. Amhar, F. Quality Test Various Existing DEM in Indonesia Toward 10 Meter National DEM. *ISPRS-Int. Arch. Photogramm. Remote Sens. Spat. Inf. Sci.* **2016**, *XLI-B4*, 111–116. https://doi.org/10.5194/isprsarchives-XLI-B4-111-2016.
22. Fenrich, K. Securing Your Control System. *Power Eng.* **2008**, *112*, . https://www.controlglobal.com/assets/knowledge_centers/abb/assets/abb_secure_control_sys.pdf (accessed on 24 January 2022).
23. Fornaro, C.; Sanna, A. Public key watermarking for authentication of CSG models. *Comput. Aided Des.* **2000**, *32*, 727–735.
24. Praun, E.; Hoppe, H.; Finkelstein, A. Robust Mesh Watermarking. In Proceedings of the 26th Annual Conference on Computer Graphics and Interactive Techniques, Broadway, NY, USA, 8–13 August 1999; pp. 49–57. https://doi.org/10.1145/311535.311540.
25. Ohbuchi, R.; Masuda, H.; Aono, M. A shape-preserving data embedding algorithm for NURBS curves and surfaces. In Proceedings of the Computer Graphics International CGI-99, Canmore, AL, Canada, 7–11 June 1999; pp. 180–187.
26. Xu, Y.; Zhang, S.; Li, J.; Liu, H.; Zhu, H. Extracting Terrain Texture Features for Landform Classification Using Wavelet Decomposition. *ISPRS Int. J. Geo-Inf.* **2021**, *10*, 658. https://doi.org/10.3390/ijgi10100658.
27. Doglioni, A.; Simeone, V. Geomorphometric analysis based on discrete wavelet transform. *Environ. Earth Sci.* **2014**, *71*, 3095–3108. https://doi.org/10.1007/s12665-013-2686-3.
28. Stankovic, S.; Djurovic, I.; Pitas, I. Watermarking in the space/spatial-frequency domain using two-dimensional Radon-Wigner distribution. *IEEE Trans. Image Process.* **2001**, *10*, 650–658. https://doi.org/10.1109/83.913599.
29. Zhang, X.; Feng, J.; Lo, K. Image watermarking using tree-based spatial-frequency feature of wavelet transform. *J. Vis. Commun. Image Represent.* **2003**, *14*, 474–491. https://doi.org/10.1016/S1047-3203(03)00047-6.
30. Malik, G. Analysis of Watermarking Techniques. *Int. J. Comput. Appl.* **2016**, *138*, 30–32.

31. Abubahia, A.; Cocea, M. Evaluating the topological quality of watermarked vector maps. *Appl. Soft Comput.* **2018**, *71*, 849–860. https://doi.org/10.1016/j.asoc.2018.07.002.
32. Shrestha, B.; O'Hara, C.G.; Younan, N.H. JPEG2000: Image Quality Metrics. In Proceedings of the ASPRS 2005 Annual Conference, Baltimore, MD, USA, 7–11 March 2005.
33. Li, Y.-M.; Wei, D.; Zhang, L. Double-encrypted watermarking algorithm based on cosine transform and fractional Fourier transform in invariant wavelet domain. *Inf. Sci.* **2021**, *551*, 205–227. https://doi.org/10.1016/j.ins.2020.11.020.
34. Matlab, "2-D DCT," Math Works. Available online: https://www.mathworks.com/help/vision/ref/2ddct.html (accessed on 24 January 2022).
35. Fazli, S.; Moeini, M. A robust image watermarking method based on DWT, DCT, and SVD using a new technique for correction of main geometric attacks. *Optik* **2016**, *127*, 964–972. https://doi.org/10.1016/j.ijleo.2015.09.205.
36. Islam, S.M.M.; Debnath, R.; Hossain, S.K.A. DWT Based Digital Watermarking Technique and its Robustness on Image Rotation, Scaling, JPEG compression, Cropping and Multiple Watermarking. In Proceedings of the 2007 International Conference on Information and Communication Technology, Bangalore, India, 15–16 December 2007; pp. 246–249.
37. Ruswiansari, M.; Novianti, A.; Wirawan, W. Implementation Discrete Wavelet Transform (DWT) And Singular Value Decomposition (SVD) on Image Watermarking. *J. Elektro dan Telekomun. Terap.* **2016**, *3*. https://doi.org/10.25124/jett.v3i1.130.
38. Gourrame, K.; Douzi, H.; Harba, R.; Ros, F.; El Hajji, M.; Riad, R.; Amar, M. Robust Print-cam Image Watermarking in Fourier Domain. In *Proceedings of the Image and Signal Processing: 7th International Conference, ICISP 2016, Trois-Rivières, QC, Canada, 30 May–1 June 2016*; Springer: Berlin/Heidelberg, Germany, 2016; pp. 356–365.
39. Woo, C.-S.; Du, J.; Pham, B. Geometric Invariant Domain for Image Watermarking. In *International Workshop on Digital Watermarking*; Springer: Berlin/Heidelberg, Germany, 2006; pp. 294–307.
40. Li, L.; Bai, R.; Lu, J.; Zhang, S.; Chang, C.-C. A Watermarking Scheme for Color Image Using Quaternion Discrete Fourier Transform and Tensor Decomposition. *Appl. Sci.* **2021**, *11*, 5006. https://doi.org/10.3390/app11115006.